01 Jan 1993

Defect Structure Of Y1-ycaymno3 And La1-ycaymno3. II. Oxidation-reduction Behavior

J. W. Stevenson

M. M. Nasrallah

Harlan U. Anderson
Missouri University of Science and Technology, harlanua@mst.edu

Don M. Sparlin
Missouri University of Science and Technology, sparlin@mst.edu

Recommended Citation

J. W. Stevenson et al., "Defect Structure Of Y1-ycaymno3 And La1-ycaymno3. II. Oxidation-reduction Behavior," *Journal of Solid State Chemistry*, vol. 102, no. 1, pp. 185 - 197, Elsevier, Jan 1993.
The definitive version is available at https://doi.org/10.1006/jssc.1993.1021

JOURNAL OF SOLID STATE CHEMISTRY 102, 185–197 (1993)

Defect Structure of $Y_{1-y}Ca_yMnO_3$ and $La_{1-y}Ca_yMnO_3$

II. Oxidation–Reduction Behavior

J. W. STEVENSON, M. M. NASRALLAH, H. U. ANDERSON, AND D. M. SPARLIN*

*Ceramic Engineering Department and *Physics Department, University of Missouri–Rolla, Rolla, Missouri 65401*

Received February 14, 1992; in revised form June 8, 1992; accepted June 24, 1992

Electrical conductivity, Seebeck coefficient, and thermogravimetric behavior of compositions in the systems $Y_{1-y}Ca_yMnO_3$ and $La_{1-y}Ca_yMnO_3$ were studied as functions of temperature and ambient oxygen activity in order to determine the mechanism of electrical transport and defect structure. Compositions in $Y_{1-y}Ca_yMnO_3$ exhibited very slight oxygen activity-dependent behavior as the ambient oxygen activity was reduced. A defect model which includes the thermally excited disproportionation of Mn^{3+} into Mn^{2+} and Mn^{4+} pairs was applied to the oxygen-activity-dependent data for $La_{0.80}Ca_{0.20}MnO_3$ and $La_{0.60}Ca_{0.40}MnO_3$. For these compositions, the experimentally observed dependence of oxygen stoichiometry, electrical conductivity, and Seebeck coefficient upon ambient oxygen activity was explained using this model.

1. Introduction

In the preceding paper, Part I (*1*), results of measurements of electrical conductivity and Seebeck coefficient in air for compositions in the systems $Y_{1-y}Ca_yMnO_3$ and $La_{1-y}Ca_yMnO_3$ were reported. In that study, a new defect model was introduced which incorporated the thermally excited disproportionation of Mn^{3+} cations into Mn^{4+} and Mn^{2+} pairs. It was found that the Seebeck data could be satisfactorily explained with this model if the Mn^{2+} were treated as a conduction site-blocking species. Simultaneous solution of the equations for fraction of sites occupied, mass balance, and electroneutrality allowed the concentrations of the three valence states of Mn to be calculated for a given composition at a given temperature. The present paper reports on measurements of conductivity, stoichiometry, and stability of these compositions as functions of the ambient oxygen activity. The defect model is extended to oxygen activity-dependent data for compositions in $La_{1-y}Ca_yMnO_3$.

2. Experimental Procedure

The procedures for specimen preparation and measurement of electrical conductivity and Seebeck coefficient can be found in the Experimental Procedure section of Part I (*1*).

The thermogravimetric apparatus consisted of a Mettler AE163 balance from which a powder specimen (in an alumina crucible) could be suspended in a vertical tube furnace that was sealed from the atmosphere. The oxygen activity in the furnace was controlled by flowing gas mixtures of N_2 and O_2 or CO_2 and forming gas at a linear flow rate of 0.5 cm/sec. Powders for thermogravimetric analysis (TGA) were coarsened

0022-4596/93 $5.00

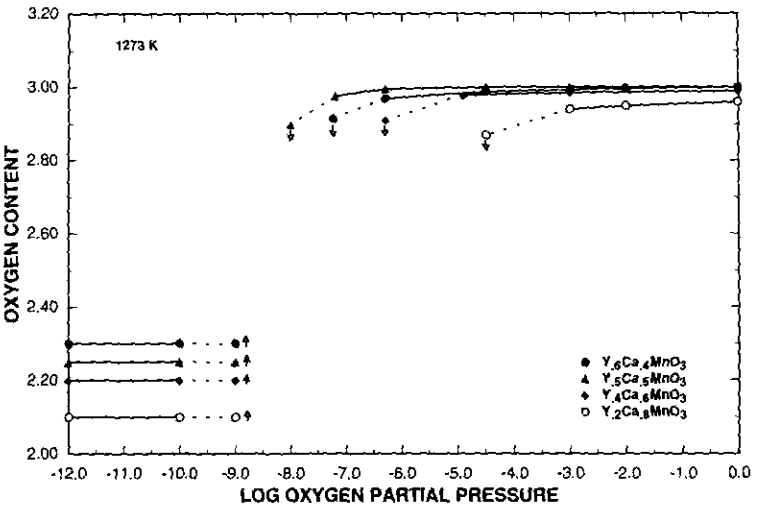

FIG. 1. Oxygen content vs log oxygen partial pressure for the indicated compositions at 1273 K. Oxygen content represents O/Mn mole ratio; oxygen partial pressure in atmospheres.

by calcination at 1273, 1373, and 1523 K (24 hr at each temperature) so that the desired mass of 15–20 g could be placed in the alumina crucible. This high-temperature calcination also ensured that any volatile inorganic impurities remaining in the specimen were removed. TGA runs were performed by equilibrating the specimen at the desired temperature in a pure oxygen atmosphere, after which the oxygen activity was reduced systematically (approximately 1 order of magnitude at a time). The equilibrium weight was recorded at each oxygen activity. After the specimen was fully reduced, reoxidation was performed to ensure that the process was reversible.

3. Results and Discussion

Thermogravimetric analysis (TGA) was performed on several compositions in $Y_{1-y}Ca_yMnO_3$ in order to determine their stability and oxygen stoichiometry as a function of oxygen activity. The TGA results for $Y_{0.6}Ca_{0.4}MnO_3$, $Y_{0.5}Ca_{0.5}MnO_3$, $Y_{0.4}Ca_{0.6}MnO_3$, and $Y_{0.2}Ca_{0.8}MnO_3$ at 1273 K are shown in Fig. 1. The effect of temperature on thermogravimetric behavior can be seen in Fig. 2, which shows TGA results for $Y_{0.6}Ca_{0.4}MnO_3$ at 1273, 1373, and 1473 K. Compositions with $y = 0.40$ or 0.50 were stoichiometric at high oxygen activity. As the oxygen activity was reduced, the oxygen content remained nearly stoichiometric until a critical oxygen activity was reached. Compositions with $y > 0.50$ were oxygen-deficient at high oxygen activity, but, as in the case of $Y_{0.6}Ca_{0.4}MnO_3$ and $Y_{0.5}Ca_{0.5}MnO_3$, the oxygen content remained nearly constant with decreasing oxygen activity until the critical activity was reached. While compositions in $La_{1-y}Sr_yMnO_3$ equilibrated to a successively lower oxygen content as the oxygen activity was lowered (2), the $Y_{1-y}Ca_yMnO_3$ compositions displayed no such oxygen-activity-dependent region. Instead, once the critical oxygen activity was reached, a dissociation reaction occurred, resulting in extensive weight loss. At sufficiently low oxygen activities, the specimen weight remained unchanged with further reduction in oxygen activity. X-ray diffraction performed on powder specimens quenched from these

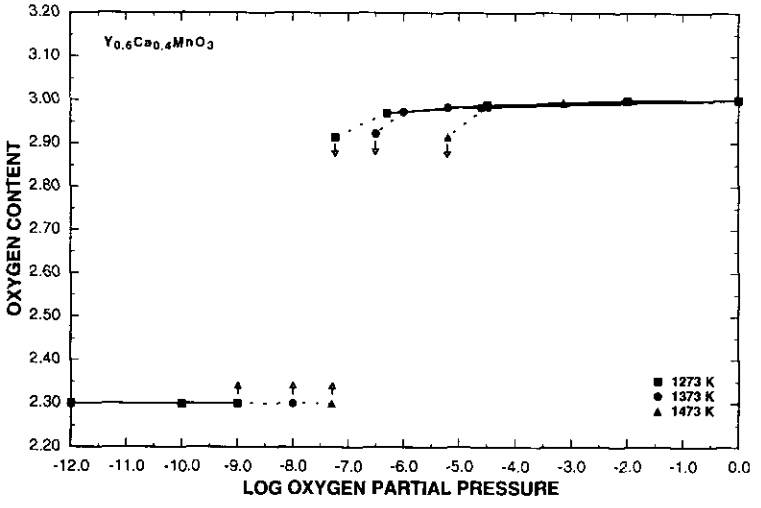

FIG. 2. Oxygen content vs log oxygen partial pressure for $Y_{0.6}Ca_{0.4}MnO_3$ at the indicated temperatures. Oxygen content represents O/Mn mole ratio; oxygen partial pressure in atmospheres.

fully reducing conditions verified that the Mn ions were reduced to a +2 valence state. For $YMnO_3$, the fully reduced products were Y_2O_3 and MnO. In compositions containing Ca, the Ca was incorporated into the MnO structure so that the final products were Y_2O_3 and a (Ca, Mn)O solid solution. The existence of this solid solution is not surprising given the similar ionic radii of Ca^{2+} and Mn^{2+} (1.00 and 0.82 Å, respectively, in 6-fold coordination (*3*)) and the fact that CaO and MnO both crystallize in the rock-salt structure.

The fully reduced state provided an important reference point. Since the valences of all the cations in the specimen were known at that point, the exact amount of each species present in the specimen could be determined. This reference state then allowed the oxygen content at other oxygen activities to be calculated.

The weight loss upon dissociation proceeded so slowly that it was only possible to follow it to completion for one composition, $Y_{0.6}Ca_{0.4}MnO_3$, at one temperature, 1473 K. For all other thermogravimetric runs, the weight loss was tracked until it became apparent that the critical oxygen activity had been reached. (Since the specimens were still losing weight at that critical oxygen activity, in the figures these nonequilibrium points are accompanied by downward pointing arrows). The oxygen activity was then reduced sufficiently to accelerate the dissociation so that the fully reduced state could be reached. The oxygen activity was then increased step-wise to find the limit of the fully reduced state. In the figures, the points at which weight gain began to occur upon reoxidation are accompanied by upward pointing arrows. During the step-wise reoxidation the weight gain began to occur at an oxygen activity somewhat lower than the critical oxygen activity for dissociation. As soon as the upper limit of the fully reduced state was determined, the oxygen activity was increased to 1 atm in order to verify the reversibility of the oxidation–reduction behavior. X-ray diffraction confirmed that, upon reoxidation, the material returned to the original single phase composition.

The observed weight gain at oxygen activities below the critical oxygen activity during stepwise reoxidation from the fully re-

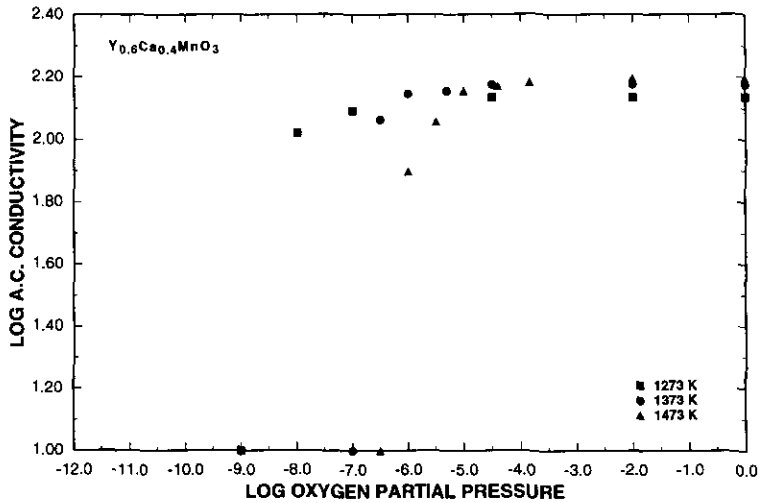

FIG. 3. Log ac conductivity vs log oxygen partial pressure for $Y_{0.6}Ca_{0.4}MnO_3$ at the indicated temperatures. Conductivity in units of S/cm; oxygen partial pressure in atmospheres.

duced state (e.g., at an oxygen activity of 10^{-9} atm. at 1273 K) was attributed to the onset of cation deficiency in the (Mn, Ca)O solid solution. Also, the phase transition from MnO to Mn_3O_4 occurs at oxygen activities between the critical oxygen activity and the upper limit of the fully reduced state.

Log a.c. electrical conductivity vs log oxygen partial pressure at 1273, 1373, and 1473 K for $Y_{0.6}Ca_{0.4}MnO_3$ is shown in Fig. 3. Log ac conductivity vs log oxygen partial pressure at 1273 K for compositions with $0.40 \leq y \leq 0.90$ is shown in Fig. 4. (Lines were added to Fig. 4 to help distinguish one

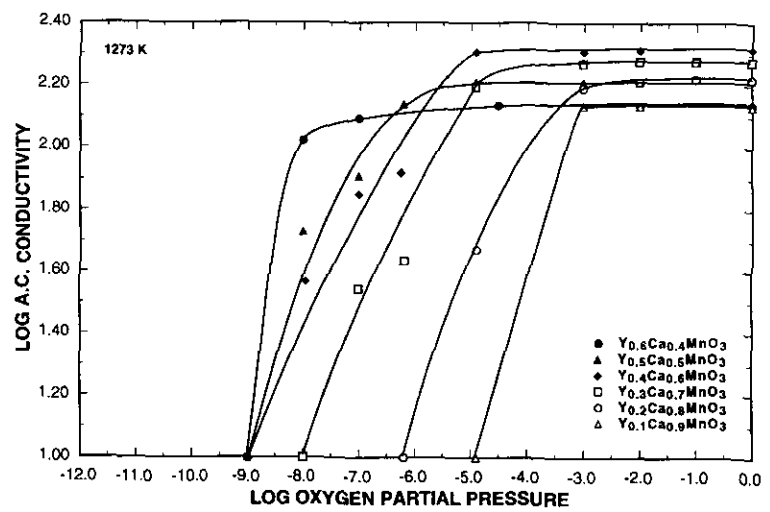

FIG. 4. Log ac conductivity vs log oxygen partial pressure at 1273 K for the indicated compositions. Conductivity in units of S/cm; oxygen partial pressure in atmospheres.

composition from another.) The electrical behavior was consistent with the TGA results in that the step-wise reduction of the oxygen activity had only a slight effect on conductivity until a critical oxygen activity was reached at which point the conductivity decreased abruptly. Upon reoxidation, the specimen conductivities returned to only 50 to 75% of their original value due to the dissociation. It was concluded from the measurements of oxygen stoichiometry and conductivity as a function of oxygen activity that a high Ca^{2+} content resulted in reduced stability upon reduction. It was also apparent that, for a given composition, stability in reducing environments decreased with increasing temperature. This temperature-dependent behavior was consistent with that of compositions in the $La_{1-y}Sr_yMnO_3$ system as reported by Kuo *et al.* (*4*).

The determination of the critical oxygen activity allowed the free energy of formation, ΔG_f°, to be calculated. Since all the products and reactants in the dissociation reaction were in the solid state except for O_2,

$$\Delta G_f^\circ = nRT(2.303) \log \left[\frac{P_{O_2}}{P_{O_2}^0}\right]. \quad (1)$$

where n is the number of moles of oxygen liberated when 1 mole of the material dissociates, P_{O_2} is the critical oxygen activity, and $P_{O_2}^0$ is the standard state of oxygen (0.1 MPa or 0.9869 atm). Since the dissociation of these materials occurred in the oxygen activity range where Mn_3O_4 is the stable Mn oxide, the free energies of formation were calculated for the following formation reaction:

$$\frac{(1-y)}{2} Y_2O_3 + \frac{1}{3} Mn_3O_4 + yCaO + \frac{(1+3y)}{12} O_2 \rightleftarrows Y_{1-y}Ca_yMnO_3. \quad (2)$$

The calculated values are listed in Table I. The free energies of formation for the compositions studied in $Y_{1-y}Ca_yMnO_3$ are considerably lower in magnitude than those for the $LaMnO_3$-based compositions. These smaller values of ΔG_f° are indicative of lower stability in the $Y_{1-y}Ca_yMnO_3$ compositions. This reduced stability may be attributed to the small size of the Y^{3+} ions.

TABLE I

CALCULATED FREE ENERGIES OF FORMATION, ΔG_f°, FOR THE INDICATED COMPOSITIONS

Composition	Temperature (K)	ΔG_f° (kJ/mole)
$Y_{0.6}Ca_{0.4}MnO_3$	1273	−32.1 ± 2.2
	1373	−31.3 ± 2.4
	1473	−26.8 ± 2.6
$Y_{0.5}Ca_{0.5}MnO_3$	1273	−36.5 ± 2.5
	1373	−32.8 ± 2.7
$Y_{0.4}Ca_{0.6}MnO_3$	1273	−35.8 ± 2.8
	1373	−33.0 ± 3.0
$Y_{0.2}Ca_{0.8}MnO_3$	1273	−31.0 ± 3.5
$La_{0.8}Ca_{0.2}MnO_3$	1373	−90.7 ± 3.9
	1473	−88.8 ± 4.2
$La_{0.6}Ca_{0.4}MnO_3$	1373	−69.0 ± 4.6
	1473	−64.1 ± 4.9
$LaMnO_3$[a]	1273	−96.9
	1373	−93.3
	1473	−83.2
$La_{0.9}Sr_{0.1}MnO_3$[a]	1273	−105.9
	1373	−100.5
	1473	−94.6
$La_{0.8}Sr_{0.2}MnO_3$[a]	1273	−116.2
	1373	−110.4
	1473	−108.3

[a] Reference (*4*).

It was important to test the defect model incorporating the disproportionation of Mn by applying it to oxygen-activity-dependent thermogravimetric and electrical conductivity data. Since the compositions in the system $Y_{1-y}Ca_yMnO_3$ did not exhibit the required oxygen-activity-dependent behavior, measurements of oxygen stoichiometry and ac conductivity as functions of ambient oxygen activity were performed on two compositions in the $La_{1-y}Ca_yMnO_3$ system ($La_{0.8}Ca_{0.2}MnO_3$ and $La_{0.6}Ca_{0.4}MnO_3$). The results of thermogravimetric analysis on

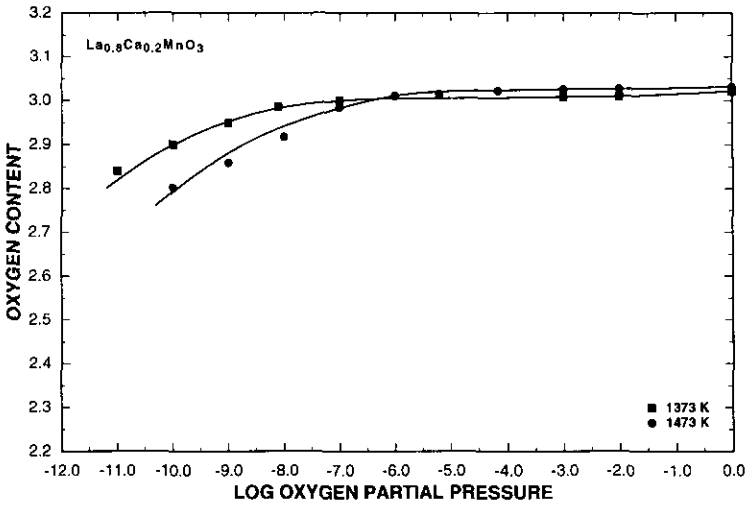

FIG. 5. Oxygen content vs log oxygen partial pressure for $La_{0.8}Ca_{0.2}MnO_3$ at the indicated temperatures. Oxygen content represents O/Mn mole ratio; oxygen partial pressure in atmospheres. The solid lines were calculated using the defect model.

$La_{0.8}Ca_{0.2}MnO_3$ at 1373 and 1474 K are shown in Fig. 5. The results for $La_{0.6}Ca_{0.4}MnO_3$ at the same temperatures are shown in Fig. 6. The presence of a significant oxygen-activity-dependent region suggests that the absence of a similar region in compositions in the system $Y_{1-y}Ca_yMnO_3$ can be attributed to the small size of the Y^{3+} ions, which apparently reduces the stability of Y-containing perovskite struc-

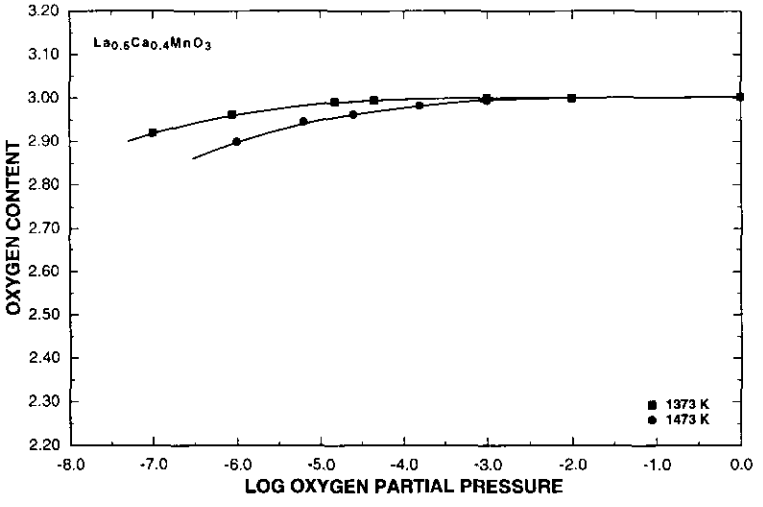

FIG. 6. Oxygen content vs log oxygen partial pressure for $La_{0.6}Ca_{0.4}MnO_3$ at the indicated temperatures. Oxygen content represents O/Mn mole ratio; oxygen partial pressure in atmospheres. The solid lines were calculated using the defect model.

tures so that they dissociate as soon as the loss of oxygen begins. The calculated free energies of formation for $La_{0.8}Ca_{0.2}MnO_3$ and $La_{0.6}Ca_{0.4}MnO_3$ are listed in Table I. For comparison, the calculated free energies of formation for compositions in the system $La_{1-y}Sr_yMnO_3$ (*2*) are also listed.

The thermogravimetric results indicated that $La_{0.8}Ca_{0.2}MnO_3$ was slightly cation deficient at high oxygen activities, while $La_{0.6}Ca_{0.4}MnO_3$ was stoichiometric. Simultaneous solution of the equations for fraction of sites occupied, mass balance, and electroneutrality (see Part I (*1*)) yielded the fully oxidized formulae below:

$$La_{0.800}(V'''_{La})_{0.007}Ca'_{0.200}Mn'_{0.202}Mn^{x}_{0.354}Mn^{\cdot}_{0.444}(V'''_{Mn})_{0.007}O_{3.020} \quad (1473\ K)$$

$$La_{0.800}(V'''_{La})_{0.007}Ca'_{0.200}Mn'_{0.200}Mn^{x}_{0.358}Mn^{\cdot}_{0.442}(V'''_{Mn})_{0.007}O_{3.020} \quad (1373\ K)$$

$$La_{0.60}Ca'_{0.40}Mn'_{0.12}Mn^{x}_{0.36}Mn^{\cdot}_{0.52}O_{3.00} \quad (1373, 1473\ K).$$

The step-wise reduction of oxygen activity initially resulted in only slight changes in the oxygen stoichiometry. The region in which the stoichiometry was essentially independent of P_{O_2} represented the "stoichiometric" region. For $La_{0.8}Ca_{0.2}MnO_3$, this region extended to oxygen activities of approximately 10^{-7} and 10^{-6} atm at 1373 and 1473 K, respectively. For $La_{0.6}Ca_{0.4}MnO_3$, the corresponding oxygen activities were approximately 10^{-5} and 10^{-4} atm. Further reduction of the oxygen activity led to a P_{O_2}-dependent oxygen deficient region which extended over several orders of magnitude of oxygen activity before dissociation of the material occurred.

The transition from slight oxygen excess to the stoichiometric composition in $La_{1-y}Ca_yMnO_3$ can be represented by the reaction (assuming that the cation vacancies are fully ionized and equally distributed over *A* and *B* sites)

$$La^{x}_{1-y}Ca'_y(V'''_{La})_{x/3}Mn'_{r'}Mn^{x}_{s'}Mn^{\cdot}_{t'}(V'''_{Mn})_{x/3}O_{3.00+x} \rightleftarrows La^{x}_{1-y}Ca'_yMn'_{r'+a'}Mn^{x}_{s'+b'}Mn^{\cdot}_{t'+c'}O_{3.00} + \frac{x}{2}O_2, \quad (3)$$

where r', s', and t' represent the initial concentrations (in mole fractions) of Mn', Mn^x, and $Mn^{\cdot}$, respectively. The variables a', b', and c' represent the change in concentration of those three valence states of Mn when the material is reduced to the stoichiometric state. Since La^{3+} and Ca^{2+} are very stable cations, only the Mn cations are assumed to change valence to maintain electroneutrality as oxygen is removed from the crystal. Equation (3) has the advantage of being quite general in that it allows any or all of the three valence states of Mn to be altered to provide charge compensation for the removal of oxygen. Equation (3) can be simplified (by elimination of those ions whose concentration remains constant) to

$$xO_O + \frac{2x}{3}V'''_M \rightleftarrows a'Mn'_{Mn} + b'Mn^{x}_{Mn} + c'Mn^{\cdot}_{Mn} + \frac{x}{2}O_2 \quad (4)$$

or

$$O_O + \frac{2}{3}V'''_M \rightleftarrows \frac{a'}{x}Mn'_{Mn} + \frac{b'}{x}Mn^{x}_{Mn} + \frac{c'}{x}Mn^{\cdot}_{Mn} + \frac{1}{2}O_2. \quad (5)$$

In order to be able to determine the formula of the material, it is necessary to know a', b', and c' as functions of the amount of oxygen removed, x. Mass balance in Eq. (5) requires that

$$a' + b' + c' = 0, \quad (6)$$

since the total amount of Mn in the crystal remains unchanged. Electroneutrality requires

$$3\left[\frac{2}{3}\right] = \frac{a'}{x} - \frac{c'}{x}. \quad (7)$$

Equations (6) and (7) allow the changes in concentration of two of the valence states of Mn to be expressed in terms of the change in concentration of the third, e.g.,

$$a' = 2x + c' \quad (8)$$

and

$$b' = -2x - 2c'. \quad (9)$$

Thus, if the relationship between c' and x is determined, values of a', b', and c' can be calculated for a given value of x. The required relationship between c' and x was obtained from experimental values of the Seebeck coefficient, Q, as a function of oxygen activity. Those values were used to obtain the fraction of available sites occupied by carriers, C, for a given oxygen activity. Since x was known at each oxygen activity (from the thermogravimetric data) it was possible to obtain C as a function of x for each composition at each temperature.

C was constant in the stoichiometric region, so

$$C_o = \frac{[Mn^x_{Mn}]}{[Mn^x_{Mn}] + [Mn^{\cdot}_{Mn}]} = \frac{(s' + b')}{[(s' + b') + (t' + c')]}, \quad (10)$$

where C_o is the experimentally determined fraction of sites occupied for the fully oxidized material. The combination of Eqs. (9) and (10) gave the required relationship for c' as a function of x:

$$c' = \frac{(2x - s')(1 - C_o) + C_o t'}{C_o - 2}. \quad (11)$$

The stoichiometric formula was calculated by substituting the degree of oxygen excess in the fully oxidized condition, x, into Eq. (11) to obtain c', after which a' and b' were obtained from Eqs. (8) and (9). The resulting stoichiometric formula at 1373 and 1473 K for $La_{0.8}Ca_{0.2}MnO_3$ was $La_{0.800}Ca'_{0.200}Mn'_{0.228}\ Mn^x_{0.344}Mn^{\cdot}_{0.428}O_{3.000}$.

Further reduction in the oxygen activity caused the stoichiometric material to become oxygen deficient,

$$La^x_{1-y}Ca'_yMn'_rMn^x_sMn^{\cdot}_tO_{3.00} \rightleftarrows La^x_{1-y}Ca'_yMn'_{r+a}Mn^x_{s+b}Mn^{\cdot}_{t+c}O_{3.00-x}(V^{\cdot\cdot}_O)_x + \frac{x}{2}O_2, \quad (12)$$

where $r = r' + a'$, $s = s' + b'$, $t = t' + c'$, and a, b, and c are the changes in the concentrations of the three valence states of Mn as the stoichiometric material loses oxygen. Equation (12) simplifies to

$$O_O \rightleftarrows \frac{a}{x}Mn'_{Mn} + \frac{b}{x}Mn^x_{Mn} + \frac{c}{x}Mn^{\cdot}_{Mn} + V^{\cdot\cdot}_O + \frac{1}{2}O_2. \quad (13)$$

The equilibrium constant for Eq. (13) is

$$K_{13} = \frac{[Mn'_{Mn}]^{a/x}[Mn^x_{Mn}]^{b/x}[Mn^{\cdot}_{Mn}]^{c/x}[V^{\cdot\cdot}_O]P^{1/2}_{O_2}}{[O_O]}. \quad (14)$$

Substitution of the concentrations in terms of mole fraction yields

$$K_{13} = \frac{(r + a)^{a/x}(s + b)^{b/x}(t + c)^{c/x}(x)P^{1/2}_{O_2}}{3 - x}. \quad (15)$$

In the oxygen-deficient region, the relationship between C and x (as determined from experimental measurement of Q as a function of oxygen activity) was highly linear so linear regression was used to generate an equation for C as a function of x. That relation was used in conjunction with the mass balance and electroneutrality relations to obtain a, b, and c as functions of x. A value for the equilibrium constant, K_{13}, was then determined from Eq. (15) using the experimentally obtained values of x as a function of ambient oxygen activity. The solid

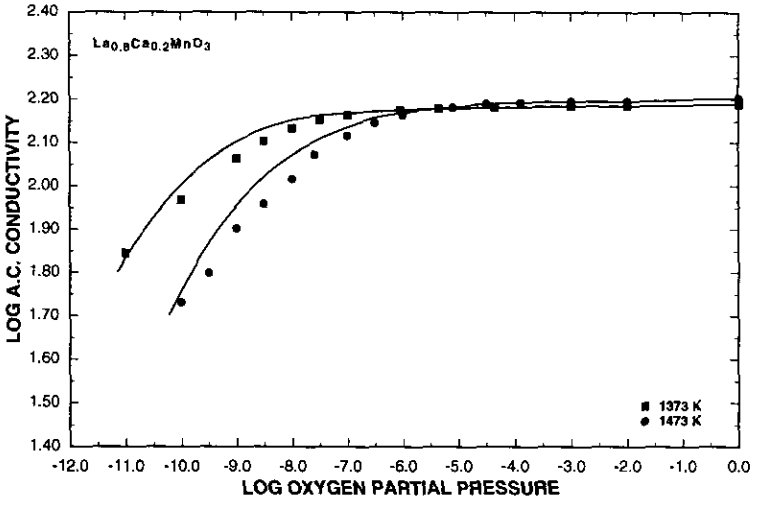

FIG. 7. Log ac conductivity vs. log oxygen partial pressure as a function of temperature for $La_{0.8}Ca_{0.2}MnO_3$. Conductivity in units of S/cm; oxygen partial pressure in atmospheres. The solid lines were calculated using the defect model.

lines in the oxygen-deficient region of Figs. 5 and 6 were calculated from Eq. (15) using the experimentally determined equilibrium constant.

Measurements of ac conductivity as a function of ambient oxygen activity were performed at 1373 and 1473 K for $La_{0.8}Ca_{0.2}MnO_3$ and $La_{0.6}Ca_{0.4}MnO_3$, as shown in Figs. 7 and 8, respectively. As in the TGA results, a significant P_{O_2}-dependent region was observed. Within this region, the conductivity decreased significantly as the degree of oxygen deficiency increased. The electroneutrality condition indicates that a change in oxygen content would alter the relative proportions of the three valence states of Mn. It is not surprising that this redistribution of valence would affect the electrical conductivity of the material.

In considering the electrical behavior in the P_{O_2}-dependent region, it was necessary to consider the expression for adiabatic polaron mobility. A carrier can only hop to an adjacent site if the site is available for conduction and if that site is not already occupied by a carrier. If a carrier was always surrounded by unoccupied available sites the mobility, μ, would be

$$\mu = \frac{eD}{kT}, \tag{16}$$

where D, the diffusion coefficient, can be expressed in terms of the lattice dimension, a, and the hopping rate, W, as

$$D = a^2W. \tag{17}$$

An additional term is required in Eq. (16) to account for the fact that some of the sites in the crystal may be either unavailable (e.g., due to site-blocking) or already occupied. It is customary to assume that mobility is proportional to the fraction of sites that are unoccupied and therefore can accept a carrier. If all sites are available for conduction, this assumption can be represented by the term $(1 - C)$. However, if noncarrier site-blocking occurs, this term must be modified. In the case of $La_{1-y}Ca_yMnO_3$, all B sites are occupied by Mn ions, so the initial fraction of B sites which can potentially participate in conduction is 1.00. This fraction must be reduced by the fraction of Mn sites which

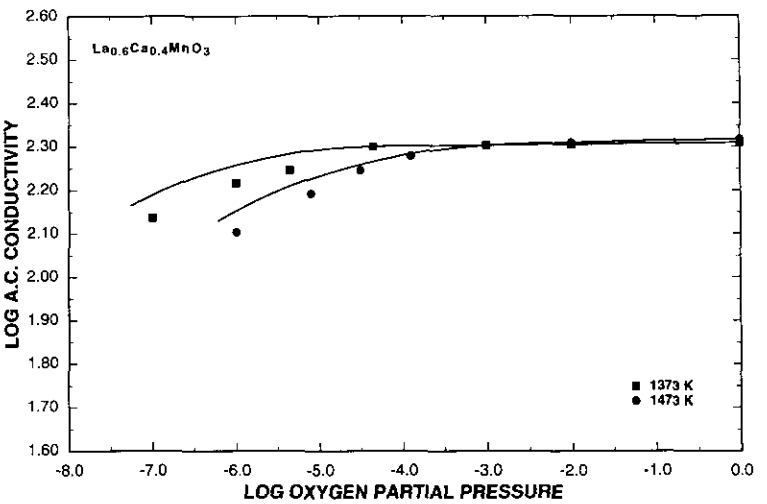

FIG. 8. Log ac conductivity vs log oxygen partial pressure as a function of temperature for $La_{0.6}Ca_{0.4}MnO_3$. Conductivity in units of S/cm; oxygen partial pressure in atmospheres. The solid lines were calculated using the defect model.

already contain a carrier (e.g., $[Mn_{Mn}^{\cdot}]$ if the carriers are holes), and by the fraction of Mn sites which are blocked, $[Mn_{Mn}']$. Thus the correction term is $(1 - [Mn_{Mn}^{\cdot}] - [Mn_{Mn}'])$, which equals $[Mn_{Mn}^{x}]$, so that

$$\mu_h = \frac{([Mn_{Mn}^{x}])ea^2W_h}{kT}. \tag{18}$$

Similarly, if the carriers are electrons, the correction term is $(1 - [Mn_{Mn}^{x}] - [Mn_{Mn}'])$, which equals $[Mn_{Mn}^{\cdot}]$, so that

$$\mu_e = \frac{([Mn_{Mn}^{\cdot}])ea^2W_e}{kT}. \tag{19}$$

Since the transport of carriers between adjacent Mn cations occurs through an exchange interaction involving the oxygen anions between those cations, the removal of oxygen from the lattice also affects carrier mobility by introducing oxygen vacancies which break the bond between adjacent Mn cations and prevent this exchange from occurring. Parris (5) used effective-medium theory to develop an expression to calculate the effect of a changing concentration of unbroken bonds on the diffusion coefficient, D,

$$D = \frac{a^2W(pd - 1)}{d - 1}, \tag{20}$$

where d is the number of dimensions of the lattice (3 for a real solid) and p is the unbroken bond concentration, which can be equated to the fraction of occupied oxygen sites per formula unit:

$$p = \frac{3 - x}{3}. \tag{21}$$

Substitution of Eq. (21) into Eq. (20) gives

$$D = a^2\left[1 - \frac{x}{2}\right]W. \tag{22}$$

Accordingly, the reduction in mobility can be approximated by replacing W with the term $[1 - (x/2)]W$, so that Eqs. (18) and (19) become

$$\mu_h = \frac{([Mn_{Mn}^{x}])ea^2[1 - (x/2)]W_h}{kT} \tag{23}$$

and

$$\mu_e = \frac{([Mn_{Mn}^{\cdot}])ea^2[1 - (x/2)]W_e}{kT}, \quad (24)$$

respectively. Since $\sigma = (NC)e\mu$, and

$$NC = \left[\frac{4}{V_c}\right]([Mn_{Mn}^{x}]) \quad (25)$$

for electron conduction and

$$NC = \left[\frac{4}{V_c}\right]([Mn_{Mn}^{\cdot}]) \quad (26)$$

for hole conduction, where N is the density of available sites and V_c is the unit cell volume (see Part I (*1*), then the conductivity is given by

$$\sigma = \left[\frac{4}{V_c}\right] \frac{([Mn_{Mn}^{x}][Mn_{Mn}^{\cdot}])e^2a^2[1 - (x/2)]W}{kT} \quad (27)$$

regardless of whether the carriers are electrons or holes.

The conductivity of the material in its oxidized state, σ_o, can be expressed as

$$\sigma_o = \left[\frac{4}{V_c}\right] \frac{([Mn_{Mn}^{x}]_o[Mn_{Mn}^{\cdot}]_o)e^2a^2W}{kT}, \quad (28)$$

where $[Mn_{Mn}^{x}]_o$ and $[Mn_{Mn}^{\cdot}]_o$ refer to concentrations in the oxidized state. Accordingly, the electrical conductivity in the oxygen deficient region can be calculated in terms of σ_o:

$$\sigma = \frac{[Mn_{Mn}^{x}][Mn_{Mn}^{\cdot}][1 - (x/2)]}{[Mn_{Mn}^{x}]_o[Mn_{Mn}^{\cdot}]_o}\sigma_o. \quad (29)$$

Thus, if the values of $[Mn_{Mn}^{x}]$, $[Mn_{Mn}^{\cdot}]$, and x were known as a function of P_{O_2}, the electrical conductivity could be calculated as a function of P_{O_2} using Eq. (29). For a given value of K_{13}, Eq. (15) fixes the degree of oxygen deficiency, x, as a function of oxygen activity. Since the model provides $[Mn_{Mn}^{x}]$ and $[Mn_{Mn}^{\cdot}]$ as functions of oxygen activity (through their dependence on x), a given value of K_{13} also fixes the electrical conductivity as a function of oxygen activity (through Eq. (29)). Therefore, if the model is correct it should be possible to find a single value of K_{13} giving a reasonable fit to both the thermogravimetric and conductivity results. The solid lines in Figs. 7 and 8 were calculated from the model. While the calculated conductivity values and the experimental data are not in perfect agreement (the experimental values decrease with decreasing oxygen partial pressure somewhat more rapidly than do the calculated values), the relatively good fit between the experimental data and the values generated by the model suggests that the defect model derived in this study is a valid representation of the defect structure of $La_{1-y}Ca_yMnO_3$ perovskites. The discrepancy between the calculated and experimental values may be due to the fact that dilute solution was assumed so that species concentration could be substituted for activity in the equilibrium expressions. Since the compositions in this study were highly doped, such an assumption is unlikely to be completely valid.

From the experimentally obtained values of K_{13} it was possible to calculate values for the free energy of formation for oxygen vacancies, ΔG_f°, from the relationship

$$K_{13} = \exp\left[\frac{-\Delta G_f^\circ}{RT}\right]. \quad (30)$$

Values of the enthalpy, ΔH_f°, and entropy, ΔS_f°, for vacancy formation were also calculated. The results of these calculations are listed in Table II. For purposes of comparison, the calculated thermodynamic values for oxygen vacancy formation in $Y_{1-y}Ca_yCrO_3$ (*6*), $La_{1-y}Sr_yMnO_3$ (*4*), and $LaCr_{1-y}Mg_yO_3$ (*7*) are also listed in Table II. The calculated enthalpies of oxygen vacancy formation for $La_{0.8}Ca_{0.2}MnO_3$ and $La_{0.6}Ca_{0.4}MnO_3$ are similar in

TABLE II

THERMODYNAMIC VALUES FOR FORMATION OF OXYGEN VACANCIES IN THE INDICATED COMPOSITIONS

Composition	Temperature (K)	Log K	ΔG_f° (kJ/mole)	ΔH_f° (kJ/mole)	ΔS_f° (J/mole)
$La_{0.8}Ca_{0.2}MnO_3$	1373	−6.41	162.0 ± 1	257 ± 20	65 ± 15
	1473	−5.74	168.5 ± 1		
$La_{0.6}Ca_{0.4}MnO_3$	1373	−5.36	140.8 ± 1	263 ± 30	89 ± 20
	1473	−4.68	131.9 ± 1		
$Y_{0.95}Ca_{0.05}CrO_3$[a]	1273	−6.85	—	189 ± 15	18
	1373	−6.31	—		
	1473	−5.79	—		
$Y_{0.90}Ca_{0.10}CrO_3$[a]	1273	−6.66	—	196 ± 15	25
	1373	−6.14	—		
	1473	−5.57	—		
$Y_{0.85}Ca_{0.15}CrO_3$[a]	1273	−6.48	—	203 ± 15	35
	1373	−5.98	—		
	1473	−5.34	—		
$Y_{0.80}Ca_{0.20}CrO_3$[a]	1273	−6.29	—	242 ± 18	67
	1373	−5.81	—		
	1473	−5.11	—		
$La_{1-x}Sr_xMnO_3$[b] $0.00 \leq x \leq 0.20$	1273–1473	—	—	360 ± 21	—
$LaCr_{1-x}Mg_xO_3$[c] $0.02 \leq x \leq 0.10$	1273–1673	—	136–169	272 ± 16	—

[a] Reference (*6*).
[b] Reference (*4*).
[c] Reference (*7*).

magnitude to those reported for the other systems.

4. Conclusion

Thermogravimetric and electrical conductivity measurements performed on $Y_{1-y}Ca_yMnO_3$ ($y \geq 0.30$) showed that as the oxygen activity was reduced at high temperatures, the oxygen stoichiometry remained essentially constant until a critical activity was reached at which point the materials abruptly dissociated. This sudden dissociation behavior in the $YMnO_3$ compositions contrasted with that in $LaMnO_3$ based compositions where a significant region of P_{O_2}-dependent oxygen stoichiometry and electrical conductivity was observed.

The defect model developed in Part I (*1*) was extended to the oxygen-activity-dependent thermogravimetric and conductivity data for compositions in $La_{1-y}Ca_yMnO_3$. Mass balance and electroneutrality relations were used in conjunction with experimental Seebeck data to calculate the oxygen stoichiometry and electrical conductivity as functions of ambient oxygen activity. The values calculated from the model were in good agreement with the experimental observations.

Acknowledgments

This research was supported by the Basic Energy Science Division and Morgantown Energy Technology Center of the United States Department of Energy.

References

1. J. W. STEVENSON, M. M. NASRALLAH, H. U. ANDERSON, AND D. M. SPARLIN, *J. Solid State Chem.*, in press.
2. J. H. KUO, "Studies of Defect Structure and Oxidation-Reduction Behavior of Undoped $LaMnO_3$, Sr-Doped $LaMnO_3$, and Mg-Doped $LaMnO_3$," Ph.D. Dissertation, University of Missouri–Rolla (1987).
3. R. D. SHANNON AND C. T. PREWITT, *Acta Crystallogr. Sect. B* **25,** 925 (1969).
4. J. H. KUO, H. U. ANDERSON, AND D. M. SPARLIN, *J. Solid State Chem.* **83,** 52 (1989).
5. P. E. PARRIS, *Phys. Rev. B* **36,** 5437 (1987).
6. G. F. CARINI II, H. U. ANDERSON, M. M. NASRALLAH, AND D. M. SPARLIN, *J. Solid State Chem.* **94,** 329 (1991).
7. B. K. FLANDERMEYER, M. M. NASRALLAH, A. K. AGARWAL, AND H. U. ANDERSON, *J. Am. Ceram. Soc.* **67,** 195 (1984).